Informatics in Medicine Unlocked 56 (2025) 101641

Contents lists available at ScienceDirect

Informatics in Medicine Unlocked

journal homepage: www.elsevier.com/locate/imu

EMG-based body–machine interface for targeted trunk muscle activation

Carolina Correia [a,*], Andrea Bandini [a,b], Silvestro Micera [a,c], Sara Moccia [a,d]

[a] The BioRobotics Institute and Department of Excellence in Robotics and AI, Scuola Superiore Sant'Anna, Pisa, Italy
[b] Health Science Interdisciplinary Research Center, Scuola Superiore Sant'Anna, Pisa, Italy
[c] Bertarelli Foundation, Translational Neuroengineering, Center for Neuroprosthetics and Institute of Bioengineering, EPFL, Genève, Switzerland
[d] Department of Innovative Technologies in Medicine and Dentistry, Università degli Studi "G. d'Annunzio" Chieti, Pescara, Italy

ARTICLE INFO

Keywords:
Body–machine interface
EMG
Human–machine interface
Machine learning
Rehabilitation
Trunk motor training

ABSTRACT

Deficits in trunk control, commonly observed in individuals with neurological conditions, can significantly impair balance, posture, and functional movements. Body–machine interfaces (BoMIs) are promising tools for trunk rehabilitation, as they can provide real-time feedback on user movements and muscle activity, allowing for continuous monitoring and guidance during motor control training. However, research on BoMIs for trunk rehabilitation is limited, and current methods often lack precision in addressing trunk muscle deficits. This work introduces a BoMI that combines trunk electromyography (EMG) and motion data to selectively modulate trunk muscle activity during motor control tasks. The system utilizes machine learning to generate personalized trunk motion trajectories based on predefined EMG profiles. Each trajectory is displayed on a screen as a moving target, which users must follow by controlling the BoMI with their trunk movements. We hypothesize that by visually guiding users to track these generated trajectories, the BoMI could evoke the EMG patterns implicitly encoded within them. Tested with neurotypical individuals, the BoMI effectively elicited the desired trunk EMG profiles, achieving a mean similarity index of 0.82 ± 0.13, a correlation coefficient of 0.95 ± 0.03, and minimal timing mismatches. These results support the feasibility of using an EMG-based BoMI for precise trunk muscle training, which could potentially assist therapists in more efficiently monitoring and adjusting patients' muscle engagement during interventions. Future work will focus on developing a control framework to dynamically adapt task difficulty to users' needs, expanding the approach to include additional trunk muscles, and evaluating its translation to individuals with trunk muscle impairments.

1. Introduction

The loss of trunk control is a common and debilitating consequence of stroke, spinal cord injury (SCI), and other neuromuscular conditions, severely compromising the ability to perform daily activities and reducing the quality of life of the affected individuals [1–3]. Deficits in trunk control are often linked to trunk muscle weakness, paralysis, and spasticity, resulting in incorrect muscle activations, insufficient segmental stiffness, and unstable posture [4,5]. Given the trunk's essential role in breathing, postural stability, and supporting limb movements, restoring trunk function emerges as one of the top priorities in rehabilitation after neurological injury [6,7].

Effective trunk rehabilitation requires not only addressing muscle strength and endurance, but also enhancing sensorimotor control to ensure proper muscle activation and coordination during dynamic tasks [8]. Body–machine interfaces (BoMIs) can play a key role in this process by providing real-time feedback and guiding users through targeted exercises that improve both muscle strength and coordination [9,10]. By converting residual muscle activity or movements into control signals for external devices, BoMIs enable interaction with various technologies while promoting motor learning [11–13].

While BoMIs have shown promising results in improving upper limb function in individuals with neurological disorders [9,14,15], their potential for trunk rehabilitation remains underexplored [16,17]. This is primarily due to the historical focus on arm function recovery for daily activities and the dominance of arm-reaching tasks in motor learning research [6,18,19]. Nevertheless, many individuals with trunk impairments, especially wheelchair users, could greatly benefit from BoMIs focused on trunk motor control training. By helping to regain trunk strength and sitting stability, BoMI-based training could improve functional arm use, facilitate transfers, and reduce pressure sores and compensatory movements [20,21].

* Corresponding author.
E-mail addresses: c.gasparpintoramoscorreia@santannapisa.it (C. Correia), andrea.bandini@santannapisa.it (A. Bandini), silvestro.micera@santannapisa.it (S. Micera), sara.moccia@unich.it (S. Moccia).

https://doi.org/10.1016/j.imu.2025.101641
Received 23 December 2024; Received in revised form 22 April 2025; Accepted 24 April 2025
Available online 6 May 2025

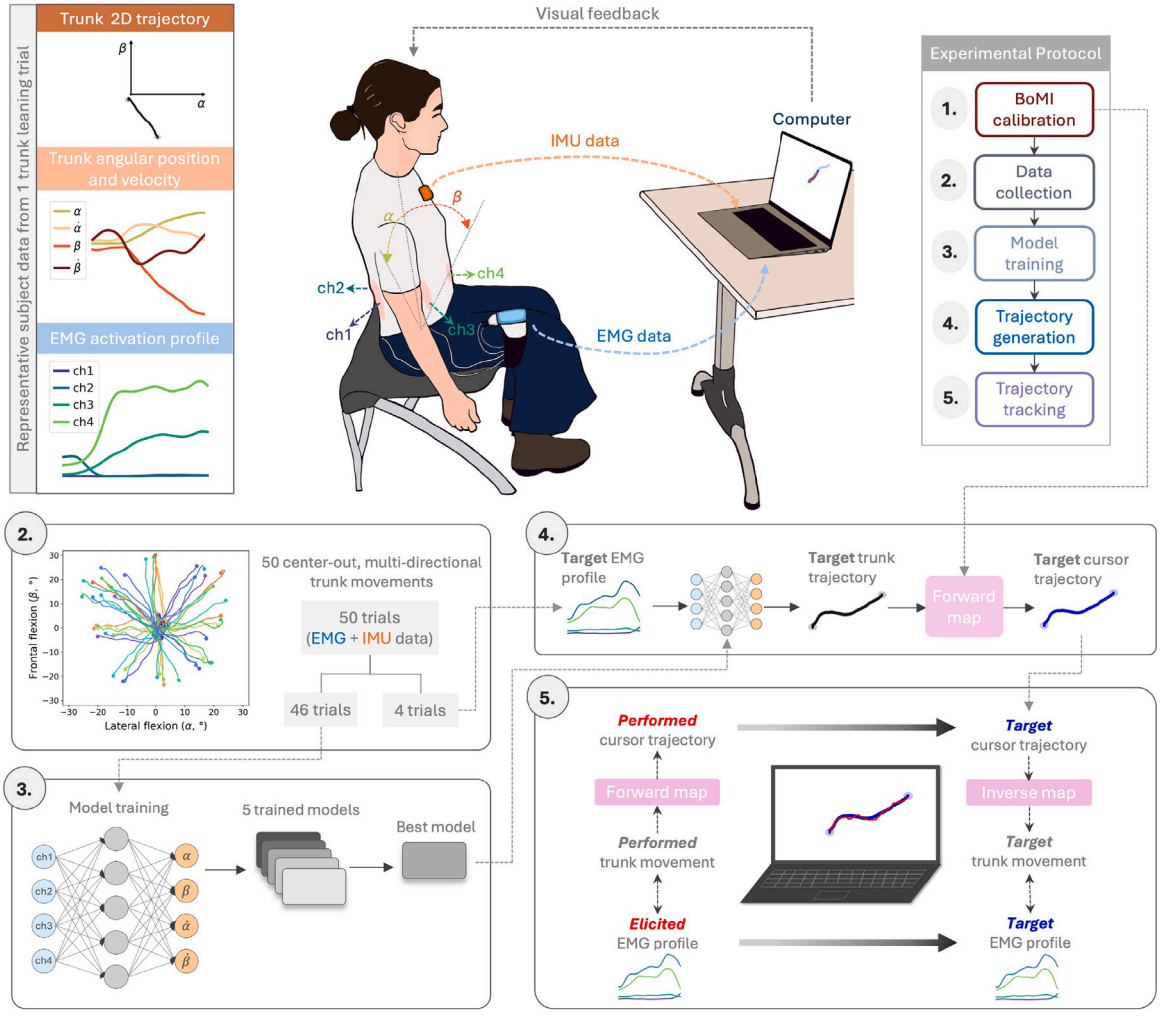

Fig. 1. Experimental setup and BoMI framework for targeted trunk muscle activation. A participant performs trunk movement tasks displayed on a screen while surface EMG activity is recorded from trunk muscles, including the erector spinae and external obliques, and an IMU captures trunk angular position and velocity. Data streams to a computer for online processing and feedback. The experimental protocol includes (1) BoMI calibration to establish the forward map linking trunk motion to cursor position, (2) sensor data collection during multi-directional trunk leaning movements, (3) neural network training to learn the subject-specific EMG-to-kinematics mapping, (4) generation of reference trunk trajectories from target EMG profiles, and (5) trajectory tracking, where the participant controls the cursor to follow the target trajectory while eliciting the target muscle activation pattern.

Among the few BoMIs developed for trunk motor training, most rely on movement-based systems that use cameras or inertial measurement units (IMUs) to track body motion and map it into cursor movements [16,17,22]. Although these systems can effectively reinforce movement patterns and improve posture, they are limited in their ability to address underlying deficits in muscle activation, such as abnormal muscle synergies or co-activation patterns common in stroke and SCI patients [23,24]. Integrating electromyography (EMG) sensors into BoMIs could offer a more precise method for targeting muscle activation, directly addressing motor control issues related to the timing, strength, and coordination of muscle contractions [25–27]. Moreover, EMG-based BoMIs have been shown to enhance voluntary muscle control in people with stroke, SCI, and multiple sclerosis, underscoring their potential to improve rehabilitation outcomes [14,15,25,26,28].

In traditional EMG-based BoMIs, the EMG amplitude of relevant muscles is mapped to cursor movement, requiring users to focus on activating specific muscles for each cursor direction [29,30]. While this method has been successful in reducing abnormal co-activations in arm muscles [15,31,32], it can be physically and mentally taxing, limiting the number of muscles that can be targeted simultaneously. Furthermore, the one-to-one mapping in proportional EMG control is not suitable for handling complex EMG patterns, which are essential for trunk stabilization and control [33]. To address these challenges, machine learning techniques, such as dimensionality reduction or regression models, offer a promising solution by simplifying the mapping of complex EMG patterns into intuitive cursor actions, thereby reducing both cognitive and physical demands [34–36]. Additionally, incorporating innovative biofeedback strategies, like linking EMG amplitude to cursor visibility or providing performance scores based on correct muscle activations, could further alleviate cognitive load and enhance user experience [14,24].

In this work, we present a BoMI that combines trunk movement and surface EMG data, aiming to achieve selective and precise activation of trunk muscles during motor control exercises. The interface consists of two main components: (1) trunk movements are mapped to control a cursor within a 2D visual interface, and (2) a user-customized, pre-trained neural network model generates target motion trajectories on the screen based on predefined muscle activation patterns (see Fig. 1). These trajectories, encoding desired muscle activations, are displayed as moving targets for users to track with their trunk movements. By shifting the focus to tracking visual targets instead of consciously activating specific muscles, this approach could reduce cognitive load and facilitate muscle engagement.

The objective of this study was to evaluate the feasibility of the BoMI in effectively eliciting the desired muscle activation patterns

through visual feedback. To achieve this, we conducted a study with neurotypical individuals who used the BoMI to track visual trajectories generated from their own trunk data. The system's performance was assessed by comparing the similarity between the target muscle activation profiles and the elicited ones. Establishing this capability is a critical step towards integrating the BoMI into rehabilitation protocols, where it could enable precise, goal-oriented trunk muscle training. By allowing therapists to define target muscle activation patterns and adapt tasks based on real-time feedback, the system has the potential to support more effective and personalized rehabilitation strategies.

1.1. Contributions

To the best of our knowledge, this is the first EMG-based BoMI designed for trunk rehabilitation. Unlike traditional EMG-based BoMIs used in clinical settings, which provide isolated, proportional feedback on individual muscle contractions without considering intermuscular coordination or movement context, our BoMI links EMG activation with functional trunk motion, enabling multi-muscle engagement during dynamic tasks. Specifically, we propose:

1. A machine learning-based approach that captures the user's EMG-motion relationship to generate personalized trunk movement exercises, adapted to each individual's neuromuscular patterns.
2. A novel biofeedback paradigm, where muscle activation is implicitly controlled through movement, rather than requiring users to explicitly contract specific muscles, fostering more intuitive engagement.
3. An integrated system that provides real-time visual feedback to guide movement execution and promote continuous, coordinated activation of multiple muscles, moving beyond traditional biofeedback focused on isolated activations or discrete EMG thresholds.

By overcoming the limitations of conventional EMG and motion-based BoMIs, our system could offer a more personalized, intuitive and functional approach to trunk motor training.

2. Methods

2.1. Sensor data acquisition and processing

We designed a BoMI that integrates two sensor modalities: surface EMG and an IMU. The IMU is responsible for detecting trunk motion and controlling the cursor in real time (explained in Section 2.2), while the EMG data informs the generation of visual trajectories for users to track (Section 2.3).

The IMU sensor (MTw Awinda, Xsens Technologies, Enschede, NL) is positioned above the subject's sternum with its x-axis aligned with the trunk length and the z-axis pointing forward. After an initial pose calibration, trunk frontal and lateral angular positions are obtained from the IMU's pitch and yaw angles, respectively. Both the trunk angular positions and velocities are acquired at 120 Hz using a ROS wrapper [37].

Surface EMG signals are recorded from four trunk muscles using a portable EMG system (Sessantaquattro+, OT Bioelettronica, Turin, IT), streaming data at 2 kHz. Bipolar pre-gelled Ag-AgCl electrodes are placed bilaterally over the lumbar erector spinae (ES) and abdominal external oblique (EO) muscles, following established guidelines [38]. These muscles were selected due to their crucial role in seated postural stabilization during trunk flexion and extension [39]. The EMG signals are preprocessed using a second-order Butterworth band-pass filter (f_c = 10–400 Hz), followed by a second-order high-pass filter (f_c = 30 Hz) to remove electrocardiographic contamination [40]. The root mean square (RMS) of the EMG signal is then computed from 150 ms time windows with a 10 ms time step, and filtered using a fourth-order low-pass filter (f_c = 20 Hz).

The interface software, implemented in Python and ROS, ensures effective parallelization and real-time synchronization of data from both sensors. Using ROS's modular architecture, we structured interface functionalities into dedicated nodes, handling tasks such as real-time data processing, data recording, and graphical interface displays.

2.2. Body-to-cursor mapping

To control the cursor, the IMU data are used to estimate the trunk angular position, $\boldsymbol{\theta} = [\alpha, \beta]^T$, where α and β represent the trunk flexion angles in the sagittal and frontal planes, respectively (Fig. 2). The trunk configuration vector, $\boldsymbol{\theta}$, is then mapped onto the visual interface through the following affine transformation:

$$\mathbf{p} = \mathbf{H} \cdot \boldsymbol{\theta} + \mathbf{b}, \tag{1}$$

where $\mathbf{p} = [p_x, p_y]^T$ denotes the cursor position, and $\mathbf{b}$ represents a position offset that aligns the trunk's neutral position with the screen's center. The matrix $\mathbf{H}$ is determined through a calibration process in which participants perform trunk flexion and extension movements to the front, back, and sides while seated. The maximum trunk range of motion (ROM) in each direction is then scaled to fit the screen dimensions, mapping frontal flexion and extension to vertical cursor movements and lateral flexion to horizontal movements.

2.3. Trunk trajectory generation

Accurately predicting movement trajectories from EMG signals remains a core challenge in fields such as prosthetics and assistive robotics [41,42]. This task requires modeling the complex, time-dependent, and often nonlinear relationship between muscle activity and motion [43]. Classical regression methods are commonly used to learn a direct mapping from EMG features (e.g. amplitudes) to kinematic outputs (e.g. joint angles) [44]. However, they typically process each time point independently, ignoring the temporal structure of the data. This limits their ability to model how past muscle activity shapes current movement, often resulting in inaccurate trajectory predictions [45].

To overcome these limitations and generate trunk trajectories from predefined EMG profiles, we adopt long short-term memory (LSTM) networks [46] — a class of recurrent neural networks specifically designed to model sequential data. Unlike conventional models, LSTMs incorporate an internal memory cell that selectively retains or discards information over time through gated mechanisms. This structure enables LSTMs to model temporal dependencies, making them particularly well-suited for capturing the dynamic relationship between EMG and movement. LSTMs have been successfully applied to decode upper and lower limb kinematics from EMG data [47–50]. Building on this foundation, we extend the use of LSTMs to trunk EMG, aiming to generate accurate, EMG-driven trunk motion trajectories.

2.3.1. Trunk modeling

To evaluate the feasibility of using LSTMs for trunk motion decoding from EMG data, we started by implementing an inverted pendulum model to simulate trunk dynamics [51]. This model approximates the trunk as a rigid body fixed at the pelvis and subject to muscle-generated forces. The pendulum's motion is described by the second-order differential equation [52]:

$$\ddot{\boldsymbol{\theta}} = \mathbf{f}_{pendulum}(\boldsymbol{\theta}, \dot{\boldsymbol{\theta}}, \boldsymbol{u}), \tag{2}$$

where the angular acceleration ($\ddot{\boldsymbol{\theta}}$) depends on angular position ($\boldsymbol{\theta}$), angular velocity ($\dot{\boldsymbol{\theta}}$), and applied forces ($\boldsymbol{u}$). These forces, applied along vertical and horizontal axes, generate torques at the pendulum's base that control its motion, similar to how muscle forces (such as those from

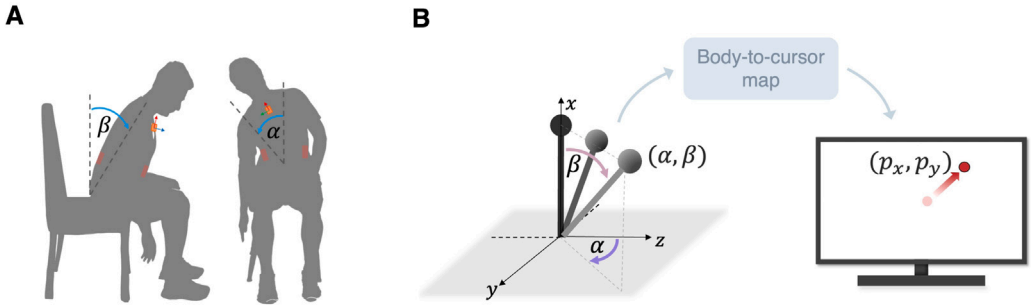

Fig. 2. Body–machine interface overview. The IMU measures trunk frontal and lateral flexion angles (A), determining the trunk's angular position, which is mapped to cursor position on the visual interface (B).

the ES muscles for trunk flexion/extension and EO for lateral bending) generate torques at the lumbar spine to control trunk movement.

This model allows us to generate synthetic data for trunk motion, providing a controlled environment to train and evaluate LSTM models (described in Section 3.1). During training, the LSTM learns to predict the pendulum's kinematic state from past input sequences that may include force, position, and velocity. However, during testing, the BoMI relies solely on EMG patterns defined by the therapist to generate trunk trajectories. Therefore, the LSTM must operate using forces (or EMG, in the human data case) as its only input.

Since the pendulum's dynamics depend on both applied forces and past states (Eq. (2)), we will test three LSTM configurations with different input combinations:

1. Forces, positions and velocities (*FPV*): this configuration provides the LSTM with complete dynamic information during training. At testing, the LSTM assumes an autoregressive structure, predicting the pendulum state, $\boldsymbol{x} = [\theta, \dot{\theta}]$, given the past d force values and predicted states.

$$\hat{\boldsymbol{x}}_t = \mathbf{f}_{LSTM_1}(\mathbf{u}_{t-1}, \ldots, \mathbf{u}_{t-d}; \hat{\boldsymbol{x}}_{t-1}, \ldots, \hat{\boldsymbol{x}}_{t-d}). \tag{3}$$

2. Forces and positions (*FP*): this structure assumes that the LSTM can infer velocity from position sequences, reducing the input complexity. At testing, the autoregressive LSTM predicts trajectories using only forces and its past position predictions.

$$\hat{\theta}_t = \mathbf{f}_{LSTM_2}(\mathbf{u}_{t-1}, \ldots, \mathbf{u}_{t-d}; \hat{\theta}_{t-1}, \ldots, \hat{\theta}_{t-d}). \tag{4}$$

3. Forces alone (*F*): this simpler configuration tests whether the LSTM can predict the pendulum's position using only the sequence of force inputs, without relying on an autoregressive structure. Although the pendulum's dynamics also depend on its state, LSTMs are powerful models that can learn complex relationships from data, potentially approximating the motion dynamics with forces alone.

$$\hat{\theta}_t = \mathbf{f}_{LSTM_3}(\mathbf{u}_t, \mathbf{u}_{t-1}, \ldots, \mathbf{u}_{t-d}). \tag{5}$$

These configurations offer a structured comparison to identify the optimal input setup for predicting pendulum trajectories, informing model decisions for subsequent human experiments using trunk EMG and IMU data.

3. Experiments and results

3.1. Synthetic data experiments

We generated 50 pendulum trajectories using the inverted pendulum model. Each trajectory was created by applying a sinusoidal force $\boldsymbol{u} = [u_\alpha, u_\beta]^T$, where u_α and u_β represent forces applied along the horizontal and vertical axes, respectively. The forces had a frequency of 10 Hz and a duration of 5 s, described by $u_i(t) = A_i \sin(\omega t + \varphi_i)$, where the amplitude A_i and phase φ_i were randomly selected within specified ranges. The pendulum started from a fixed initial position and velocity of zero. For each trajectory, we recorded the forces, angular position, and angular velocity.

The prediction model architecture consisted of stacked LSTM layers followed by a dense layer with ReLU activation to account for nonlinear dependencies. Data preprocessing involved normalization (subtracting the mean and dividing by the standard deviation (SD)), segmentation into windows based on the desired time-window and window step, and random shuffling of input–output pairs.

To determine the optimal model configuration and hyperparameters, we conducted a grid search, varying the input (*F*, *FP*, *FPV*), the number of LSTM layers (2, 3), the number of neurons in the hidden (64, 128, 256) and dense (16, 32, 64) layers, and the prediction window length (0.5, 1, 1.5 s). Each combination underwent 5-fold cross-validation, with 80% of the data allocated for training and 20% for testing in each fold. Models were trained for 5000 epochs using ADAM optimization and mean squared error (MSE) loss, with dynamic learning rate starting at 0.001 and reducing by a factor of 0.5 after 200 epochs without improvement. All models were implemented in Pytorch and trained on an NVIDIA GeForce RTX-3070 GPU. The average MSE for training and testing was recorded for each combination, and model comparisons were performed using an unpaired t-test or Mann–Whitney U test, depending on the MSE normality assessed via the Shapiro–Wilk test, with α set at 0.05.

3.2. Model selection

The grid search results revealed that the most effective LSTM model for predicting pendulum trajectories incorporated both kinematic and force data as input, significantly outperforming models that used force alone (*F* vs. *FP*: $U = 475$, $p < 0.001$; *F* vs. *FPV*: $U = 375$, $p < 0.001$, Mann–Whitney U test). As shown in Fig. 3A, longer prediction windows led to a reduction in MSE for force-only models, while no significant improvement was observed for more complex models. This suggests that models with richer input features are less sensitive to the window length, favoring *FP* or *FPV* models with shorter, 0.5–1 s windows.

Since no significant differences in MSE were found between models with *FP* and *FPV* inputs ($U = 1445$, $p = 0.932$, Mann–Whitney U test), we further examined their trajectory generation in autoregressive mode to assess error propagation. As seen in Fig. 3B, providing 1-s input sequences of past forces, position, and velocities minimized error accumulation compared to other configurations, suggesting this as the optimal configuration for our final model.

No consistent differences were found across hyperparameter configurations, except during training, where increasing the hidden dimension from 64 to 256 neurons and reducing the number of LSTM layers from 3 to 2 significantly improved performance. Based on these findings, the final model architecture included 2 LSTM layers with 256 neurons per hidden layer, a dense layer with 64 neurons, a 1-s prediction window, and input features combining trunk angular position, angular velocity, and EMG data.

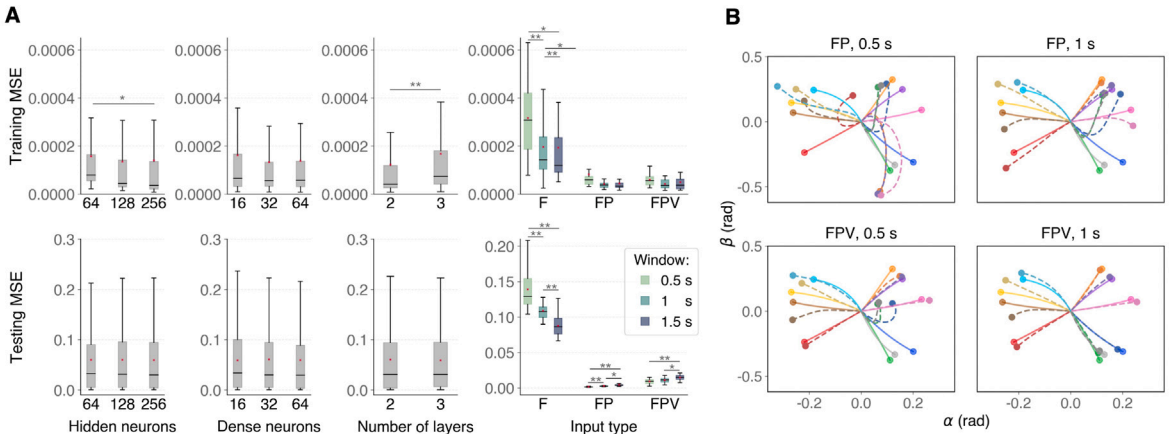

Fig. 3. Influence of LSTM model parameters on pendulum motion prediction accuracy. (A) Average training and testing MSE for various model parameters. (B) Example of target (solid lines) and predicted (dashed lines) pendulum trajectories for four input and window size combinations. F: force, FP: force and position, FPV: force, position and velocity.

3.3. Human data experiments

Six neurotypical individuals (two females and four males, aged 28.8 ± 1.3 years old) with no history of musculoskeletal or neurological disorders were enrolled in the study. The study protocol comprised four stages: (1) data collection, (2) model training, (3) trajectory generation, and (4) trajectory tracking (see Fig. 1). During stages (1) and (4), participants were instructed to sit with the back straight and unsupported, relaxed arms at the sides, and legs at a 90-degree angle. This neutral posture served as the starting position before initiating any trunk movement. Tape markers were placed on the floor to ensure consistent posture throughout the experiments.

In the data collection stage, participants performed 50 self-paced, center-out trunk movements, each lasting 5 s with a 5-s rest in between. These movements involved tilting the trunk forward, backward, laterally, or at any oblique angle, allowing participants to explore their range of motion while maintaining balance. To ensure the movements remained within the sagittal and frontal planes, participants were instructed to avoid trunk axial rotation. IMU and EMG data were recorded, resampled at 100 Hz, and reshaped into a $50 \times 500 \times 8$ array (50 movements, 500 samples, 8 dimensions: 4 IMU and 4 EMG features). Four of these movements were set aside for the trajectory generation phase. These were pseudo-randomly selected to maximize the cumulative workload of one trunk muscle at a time [53], ensuring that each movement predominantly targeted a specific muscle.

The training data were then windowed, normalized, paired with corresponding outputs, and shuffled. This resulted in an input array of size $N \times d \times 8$ and output array of size $N \times 4$, where N was the number of samples and $d = 100$ the window length. Five LSTM models were trained per participant, following the procedure outlined in Section 3.1. Model performance was evaluated using training and validation MSE, with the best model selected based on the lowest MSE on the validation set.

In the trajectory generation stage, the four reserved EMG patterns were input into the LSTM model, which generated four trunk motion trajectories in autoregressive mode. Each predicted trunk trajectory was mapped to the screen as a moving target, following a predefined path with a set velocity profile (see Fig. 1B). Participants initiated each tracking task from a neutral position and, after holding it for 3 s, the target began moving along the reference path. They were instructed to closely track the moving target by controlling the interface cursor with their trunk. On the screen, participants could see both the time elapsed since the task began and their own path overlaid on the reference path for comparison. The task ended when the participant's cursor reached the end of the reference path. Each participant completed a total of 20 trials, each consisting of tracking all 4 generated trajectories presented in a random order. These trials were divided into 4 blocks of 5 trials each, with breaks between blocks.

Note that during this phase, cursor movement was controlled by IMU data, while EMG data and relevant interface parameters were recorded for evaluation of the elicited muscle activations during trunk movements.

3.4. Human data analysis

The primary outcome of this study was the similarity between the target and elicited EMG profiles, reflecting the BoMI's ability to guide trunk muscle activation. Secondary measures, such as trajectory generation accuracy and trajectory tracking performance, were also assessed to determine their contribution to eliciting desired EMG profiles.

The BoMI's trajectory generation accuracy was evaluated by computing the MSE between the predicted and true trunk trajectories for each participant and task. Participant performance in tracking moving targets was evaluated using task completion time, cursor tracking error, and the balanced integration score (BIS). The BIS combines speed and accuracy by subtracting the standardized task completion time from the standardized tracking error [54]. Trunk kinematics were assessed through the maximum trunk ROM during calibration and, during tracking tasks, by analyzing the error between the generated and experimental trunk motion trajectories. These errors, along with cursor tracking errors, were quantified using the dynamic time warping distance (DTWD), which measures the similarity between time-series data while accounting for variations in movement timing and speed [55–57].

To evaluate the effectiveness of the BoMI in guiding participants to achieve predefined trunk muscle activations, we examined the similarity between the target and elicited EMG activation profiles using three metrics:

- **Correlation coefficient (R)**: This metric quantifies the linear relationship between two EMG signals, ranging from −1 (perfect negative correlation) to 1 (perfect positive correlation), with 0 indicating no correlation. R captures the shape and trend alignment of signals but does not account for amplitude variations or temporal misalignment [58]. Thus, it is useful for assessing overall pattern alignment, but less suitable when signals differ in scale or timing.
- **Similarity index (SI)**: The SI measures the degree of alignment between the EMG profiles by comparing their direction and relative amplitudes across all channels [59]. It is defined as:

$$\mathrm{SI} = \frac{\sum_{i=1}^{n} (EMG_{\mathrm{exp},i} \cdot EMG_{\mathrm{ref},i})}{\|EMG_{\mathrm{exp}}\| \cdot \|EMG_{\mathrm{ref}}\|}, \tag{6}$$

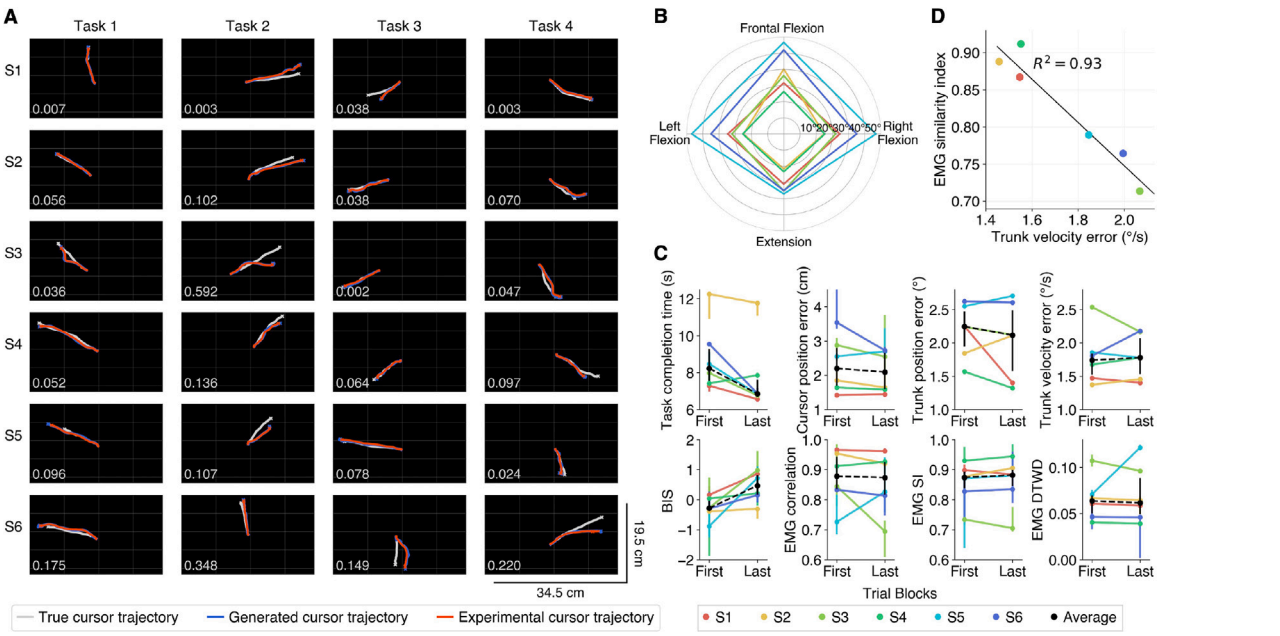

Fig. 4. Performance in the trajectory tracking task. (A) True, generated and experimental cursor trajectories for each participant and task, with the MSE between true and generated trunk trajectories on the bottom left corner. (B) Maximum trunk ROM across participants. (C) Average changes in cursor tracking performance, trunk kinematics error, and trunk EMG profile similarity from the first to the last trial blocks. (D) Correlation between error in trunk angular velocity and EMG profile similarity index.

where n is the number of EMG channels, EMG_{exp} is the elicited (experimental) EMG profile, and EMG_{ref} is the target EMG profile. SI values range from 0 to 1, with 1 indicating perfect alignment. Unlike R, SI accounts for both shape and magnitude, making it suitable for assessing whether EMG profiles match in both patterns and relative signal amplitudes. However, like R, it assumes EMG profiles have the same duration.

- **Dynamic time warping distance**: DTWD measures the temporal alignment of signals by optimally warping one signal to match another, minimizing differences caused by timing misalignments or signal length variations. Smaller DTWD values indicate higher similarity in terms of both signal shape and timing. This metric has been effectively used to compare EMG profiles, making it well-suited for rehabilitation tasks where timing variations are common and precise alignment may be crucial [60].

Experimental EMG profiles were derived by averaging the 20 profiles recorded across trials for each tracking task. Baseline EMG activity was removed by subtracting the mean activity during the 1-s period preceding task initiation. To compute R and SI, EMG profiles were resampled and normalized to the total movement time (0%–100% with 0.5% increments) to account for varying signal durations. All metrics were evaluated for each task and trial across participants.

Lastly, a correlation analysis was conducted to assess the influence of task performance on the elicitation of target EMG profiles. We hypothesized that improved cursor tracking performance would be associated with higher EMG similarity scores. Furthermore, we anticipated that greater trunk movement error would negatively impact muscle activation and decrease the alignment with target EMG profiles.

3.5. Results

3.5.1. Trajectory generation

Fig. 4A illustrates the trunk trajectories generated by each participant's model, using four distinct EMG profiles to produce four corresponding tasks, projected onto the screen. The mean MSE values between predicted and true trunk trajectories revealed significant variability among participants. Overall, participants S1, S2, S4 and S5 demonstrated accurate model predictions, with the model-generated trajectories in blue closely following the true trajectories in gray. The lowest average MSE of 0.014 ± 0.022 across tasks was observed for S1, reflecting model consistency and accuracy in trajectory generation. In contrast, participants S3 and S6 exhibited substantial variability and higher average MSE values across tasks. Specifically, S3 had a mean MSE value of 0.179, mainly due to a significant error in task 2, while S6 recorded the highest average MSE of 0.220 ± 0.313.

3.5.2. Trajectory tracking

From the first to the last trial block, participants showed an overall improvement in trajectory tracking performance (Fig. 4C). On average, across all tasks, task completion time decreased from 8.5 to 6.8 s, with a 1.8-s lag behind the 5-s reference trajectory. This increase in speed was accompanied by a slight improvement in cursor tracking precision, with DTWD decreasing marginally by 0.13 cm. Consequently, BIS increased, reflecting a shift from prioritizing tracking precision at the cost of speed (negative BIS) to a more balanced strategy, where participants focused on completing tasks faster while maintaining similar accuracy.

Changes in trunk kinematics varied across participants, showing no consistent trends. The average trunk position error slightly decreased from 2.25° to 2.12° in the final trial block, indicating a minor improvement in positional control. Trunk velocity error remained relatively stable across trial blocks, with a median of 1.78°/s in the final block. Notably, participants S5 and S6, who exhibited the highest trunk position errors, had considerably larger ROM limits compared to S4, who demonstrated the lowest trunk position errors. Specifically, S5 and S6 reached maximum frontal flexion above 50° during calibration, while S4 remained within 25° in all trunk motion directions (Fig. 4B). This increased trunk ROM in S5 and S6 likely led to more demanding movements and higher difficulty during tracking tasks, which could have contributed to higher kinematics and cursor tracking errors.

3.5.3. EMG profile similarity

Overall, the interface-generated trajectories successfully elicited the desired EMG profile, accurately targeting the intended muscle and activation pattern. As shown in Table 1, the correlation coefficient (R) values for the target muscles were consistently high across tasks and participants, with an average R of 0.95 ± 0.03. These strong R values indicate a close alignment between the target (EMG_{ref}) and elicited

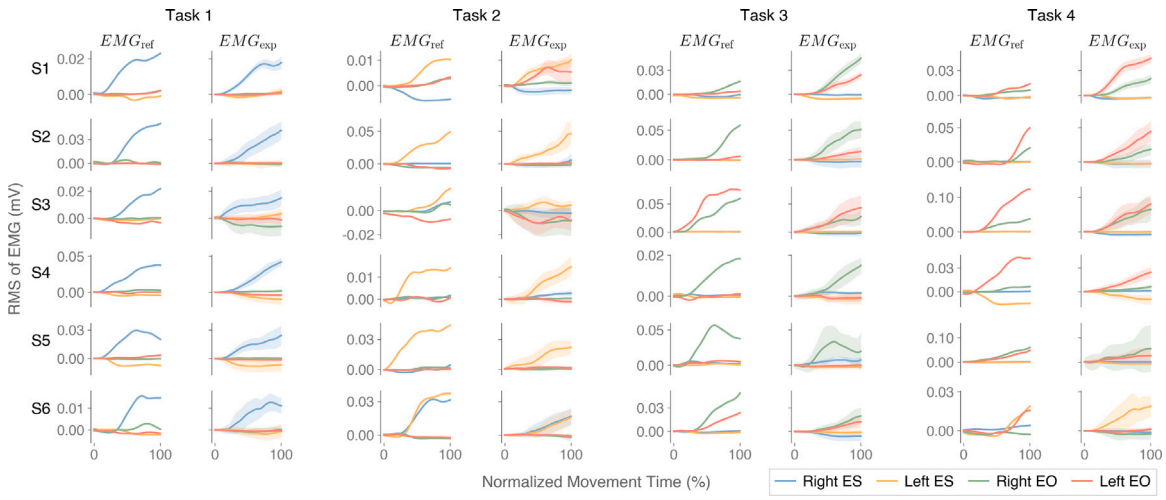

Fig. 5. Reference and experimental EMG profiles from four trunk muscles, for each participant and task, represented as function of normalized movement time. The experimental EMG profile is the average profile across all trials, with the SD represented as the shaded area around the mean.

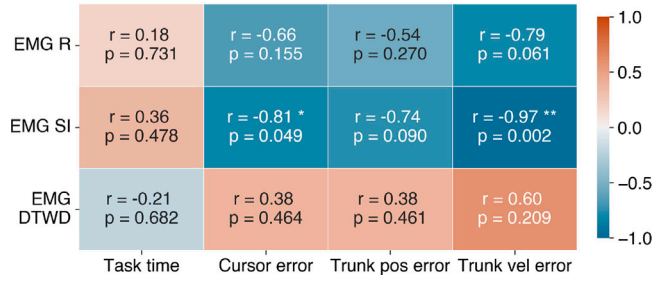

Fig. 6. Pearson correlations between EMG profile similarity metrics and user performance during target tracking task.

(EMG_{exp}) muscle activation profiles, as seen in Fig. 5. For example, Task 1, targeting the right ES muscle, had the highest R of 0.96, reflecting strong consistency in muscle activation and shape matching. Participants S1, S2, and S4 exhibited the highest R values (>0.95), while S3 showed the lowest R (0.91 ± 0.07), likely due to larger errors in the generated trajectory in Task 2.

The mean SI of 0.82 ± 0.13 further supports the strong overall similarity between EMG profiles. As with R, S1, S2, and S4 showed the highest SI values (>0.86), while S3 had the lowest (0.71 ± 0.25). However, the SI also revealed subtle differences in profile amplitude. For instance, in Task 2, although participant S1's left ES muscle closely matched the target shape (R = 0.97), the left EO muscle activated more quickly and with greater amplitude than in the target profile, resulting in a reduced SI of 0.73. In general, Tasks 1 and 3 showed higher SI and R values compared to Tasks 2 and 4, which could suggest more effective control of right-side trunk muscles relative to the left.

Finally, the low DTWD values (mean: 0.05 ± 0.02 mV) indicated minimal timing mismatches across tasks, particularly for simpler profiles like Tasks 1 and 2. Tasks 3 and 4 showed slightly higher DTWD values (mean: 0.11 mV), indicating subtle timing shifts where elicited profiles occasionally lagged or advanced relative to the reference signals. For example, in participants S3 (Task 4) and S5 (Task 3), higher DTWD values were observed, with greater temporal mismatch for S3 and increased variability in S5's EO muscle response. These higher DTWD values in Tasks 3 and 4 may result from the increased complexity and physical demand of controlling backward/lateral trunk tilts, as compared to forward tilts.

3.5.4. Correlation analysis

The correlation analysis revealed that SI was the EMG similarity metric most strongly associated with user performance in the target tracking tasks (Fig. 6). Specifically, SI exhibited a strong negative correlation with cursor position error (r = −0.81, p = 0.049) and a very strong negative correlation with trunk velocity error, as measured by DTWD (r = −0.97, p = 0.002). These findings suggest that better performance in the tracking task, both in terms of cursor accuracy and trunk motion, may be linked to more consistent muscle activation patterns and better alignment with the desired EMG profiles. This relationship is further illustrated in Fig. 4D, where the correlation between EMG SI and trunk velocity error is depicted. No significant correlations were found for R and DTWD of EMG across the performance metrics, indicating its weaker association with task performance.

Table 1
EMG similarity between target and elicited EMG profiles across participants and tasks. DTWD is in mV.

Metric	Participant	Task				Mean (SD)
		1	2	3	4	
R	S1	0.98	0.97	0.97	0.97	0.97 (0.01)
	S2	0.98	0.94	0.96	0.96	0.96 (0.02)
	S3	0.94	0.80	0.95	0.93	0.91 (0.07)
	S4	0.96	0.99	0.98	0.97	0.98 (0.01)
	S5	0.94	0.95	0.91	0.89	0.92 (0.03)
	S6	0.97	0.94	0.96	0.94	0.95 (0.02)
	Average	**0.96**	**0.93**	**0.96**	**0.94**	**0.95** (0.03)
SI	S1	0.98	0.73	0.87	0.89	0.87 (0.11)
	S2	0.97	0.92	0.88	0.79	0.89 (0.08)
	S3	0.74	0.32	0.92	0.87	0.71 (0.25)
	S4	0.93	0.88	0.91	0.93	0.91 (0.02)
	S5	0.88	0.92	0.81	0.55	0.79 (0.16)
	S6	0.85	0.83	0.85	0.52	0.76 (0.16)
	Average	**0.89**	**0.77**	**0.87**	**0.76**	**0.82** (0.13)
DTWD	S1	0.03	0.04	0.08	0.05	0.05 (0.02)
	S2	0.04	0.05	0.04	0.05	0.04 (0.01)
	S3	0.05	0.08	0.06	0.08	0.07 (0.02)
	S4	0.02	0.02	0.03	0.02	0.02 (0.01)
	S5	0.03	0.04	0.07	0.13	0.07 (0.05)
	S6	0.04	0.04	0.05	0.05	0.04 (0.01)
	Average	**0.04**	**0.05**	**0.06**	**0.06**	**0.05** (0.02)

4. Discussion

This study evaluated the feasibility of an EMG-based BoMI designed to selectively modulate trunk muscle activity during motor control exercises. Our primary aim was to determine whether the developed interface could effectively guide neurotypical individuals to achieve

specific EMG activation patterns in their trunk muscles by tracking interface-generated trajectories.

Our results demonstrate that the BoMI successfully elicited the desired trunk EMG activation patterns, with an average SI of 0.82 ± 0.13, correlation coefficient of 0.95 ± 0.03 and DTWD of 0.05 ± 0.02 mV. These values indicate a high degree of similarity between the target and elicited EMG profiles, consistent with values reported in the literature for neurotypical individuals [57,58,61–63]. For example, SI values between 0.82 and 0.99 have been observed during simple flexion–extension of lower limbs [59], whereas lower SI values (0.63 ± 0.15) have been reported for more complex trunk motions [64]. These comparisons highlight the inherent challenge of achieving precise trunk muscle control but also underscore the success of our system in addressing this complexity.

The strong correlation between task performance and EMG similarity further supports the BoMI's effectiveness. Participants who demonstrated better precision in controlling cursor position and trunk velocity tended to exhibit EMG profiles more closely aligned with the target ones. This emphasizes the importance of velocity feedback in task design, as it plays a critical role in eliciting accurate muscle activation. Unlike conventional EMG-based BoMIs, which focus on reaching a static target by matching EMG amplitudes [15,30], our approach tracks a moving target with a set velocity profile, enabling more precise control over both amplitude and timing of muscle activity. This nuanced control could be especially advantageous for trunk control training, where coordinated muscle activity is essential for maintaining balance.

A key feature of the BoMI is the use of an LSTM model to learn the relationship between trunk EMG signals and motion, enabling the generation of personalized trajectories tailored to individual capabilities. The model's performance was validated through both synthetic simulations and real-world experiments. Notably, the LSTM achieved a median MSE of 0.067 across participants, effectively generating trunk movement trajectories from EMG profiles. While the synthetic example showed minimal errors, some deviations were observed in real-world trajectories. These discrepancies were expected due to the inherent complexity of human trunk motion compared to the simplified pendulum model, as well as sensor data noise and partially captured trunk dynamics. Future efforts will aim to refine trajectory generation by utilizing enhanced computational resources and integrating additional sensors to improve the accuracy of trunk kinematic estimation.

Variability in trajectory generation and tracking performance was also observed across participants, potentially influenced by differences in trunk ROM. As described in Section 2.2, the cursor was controlled through frontal and lateral trunk movements, mapped to the screen based on the maximum trunk ROM recorded during calibration. We observed that trunk ROM limits varied among participants, not only due to their physical capacity but also their confidence in fully exploring their ROM. Participants who leaned further during calibration were required to perform more demanding movements in the trajectory tracking task, leading to posture adjustments—such as lifting feet or rotating the trunk—that affected task performance and trunk EMG response. Although posture was monitored visually and with an IMU placed above the sternum, additional IMU sensors on the lower back and shoulders could more effectively capture and correct posture variations, helping to control axial trunk rotations, lumbar and cervical curvatures, and pelvis tilt.

In the trajectory tracking task, participants demonstrated improvements in task completion time and BIS, suggesting faster and more efficient movements without compromising accuracy. However, EMG profile similarity remained stable, which was expected given the participants' intact motor control and the study's focus on guiding muscle activation through biofeedback rather than inducing neuromuscular adaptation. While this approach establishes a foundation for motor training, it does not yet integrate key motor learning principles, such as progressive overload, task variability, and repeated practice, which are essential to drive muscle strengthening, endurance gains, or long-term changes in EMG activity [65]. Therefore, to translate the BoMI into an effective tool for trunk rehabilitation, the protocol must be expanded to include multiple sessions of repetitive, goal-directed exercises, delivered through an adaptive, closed-loop biofeedback system capable of dynamically adjusting to user performance.

In this context, the EMG similarity metrics used in this study could serve as real-time indicators of patient performance, guiding rehabilitation goals, task adaptation and feedback delivery. By quantifying deviations from neurotypical EMG patterns, these metrics could help clinicians monitor patient progress toward target EMG profiles and identify muscle groups requiring intervention. For example, a post-stroke patient with hemiparesis may exhibit impaired trunk control, with reduced muscle activation on the paretic side and compensatory over-recruitment on the contralateral side. Initially, their EMG similarity to a neurotypical reference pattern may be low, reflecting these motor deficits. In response, the BoMI could adjust exercise difficulty by modulating cursor speed, trajectory complexity, or movement amplitude, ensuring an appropriate level of challenge throughout recovery. In parallel, real-time corrective feedback (e.g., auditory or color-coded visual cues) could promote more symmetrical trunk recruitment by encouraging activation of under-recruited muscles and discouraging compensatory strategies. Over time, this approach could gradually shift the patient's EMG patterns toward more balanced and functional activation, helping to restore trunk motor control.

In our study, muscle activation profiles were derived from user-specific EMG data, allowing us to validate trajectory generation through direct comparison with true trajectory data. In clinical settings, however, therapists will select EMG profiles based on patient needs, specifying parameters such as target trunk muscles, activation timing, and intensity. The BoMI would then match these inputs to an appropriate EMG profile from a predefined dictionary of profiles, built with prototype data from neurotypical individuals. This target profile would then be fed into a patient-specific model to generate the corresponding exercise. While this workflow enables a flexible and therapist-driven approach, applying it to patient populations might introduce several challenges.

Unlike neurotypical users, patients often exhibit highly variable and inconsistent EMG and kinematic signals due to spasticity, muscle weakness, compensatory strategies, and fatigue. These factors can degrade data quality, weaken the EMG-motion relationship, and limit the model's generalizability. To address these issues, future clinical implementations may require extended calibration sessions to capture a wider range of patient-specific patterns, longer rest periods to mitigate fatigue effects, and advanced EMG processing techniques to filter out artifacts from involuntary activations and compensatory movements [66,67]. Moreover, as patients adopt new motor strategies during recovery, the model should undergo regular recalibration via incremental learning [68], allowing continuous updates to the EMG-motion relationship and ensuring that task generation remains responsive to their evolving neuromuscular control.

Lastly, the current system is designed to be relatively cost-effective and simple compared to conventional motion capture or robotic rehabilitation setups, relying only on wearable IMU and EMG sensors. However, there is room to further improve portability and usability. Future iterations could replace the current desktop setup by a compact, GPU-enabled embedded system, reducing hardware demands and enhancing portability. To simplify clinical deployment, the system could also include a pre-configured workflow to automate calibration and task generation, requiring minimal technical expertise. Additional improvements, such as a more intuitive graphical interface, predefined task templates for common rehabilitation goals (e.g., strengthening weak muscles), and automated performance reports, could further streamline the BoMI operation in clinical settings.

Future research should explore the inclusion of additional trunk muscles and degrees of freedom, such as axial rotations, to provide a more comprehensive assessment of trunk motor control. Recording

both outward and return movements, or incorporating hold positions, could further enrich the evaluation. Additionally, embedding gaming features within the interface, rather than relying solely on simple cursor control, could enhance user engagement and adherence to rehabilitation tasks. While the current study shows promising results, limitations such as the small sample size may restrict the generalizability of the findings. As this was an initial feasibility study, a power analysis was not conducted, and the results should be interpreted with caution. Further studies with larger and more diverse populations will be necessary to validate the BoMI's utility across a broader range of individuals and conditions.

5. Conclusion

This study demonstrates the feasibility of using an EMG-based BoMI to guide trunk muscle activation during motor control exercises. The system successfully elicited the desired EMG profiles, highlighting its potential for targeted trunk muscle training. Future work will focus on developing a control framework to adapt the BoMI based on EMG feedback, incorporating a wider range of trunk muscles and movements, and exploring its application in clinical settings to enhance rehabilitation outcomes.

CRediT authorship contribution statement

Carolina Correia: Writing – review & editing, Writing – original draft, Visualization, Validation, Software, Methodology, Investigation, Formal analysis, Data curation, Conceptualization. **Andrea Bandini:** Writing – review & editing. **Silvestro Micera:** Writing – review & editing, Validation, Resources, Project administration. **Sara Moccia:** Writing – review & editing, Visualization, Validation, Supervision, Resources, Project administration, Methodology, Investigation, Conceptualization.

Ethical statement

This study was conducted in accordance with the Declaration of Helsinki and received approval from the Ethics Committee of Scuola Superiore Sant'Anna (approval no. 45/2023). Prior to participation, all individuals provided written informed consent.

Funding

This work was supported in part by the Italian Ministry of University and Research through the National Operational Programme on Research and Innovation (CCI: 2014IT16M2OP005) and the Italian Fund for Applied Sciences (FISA, grant no. FISA2022-00696).

Declaration of competing interest

The authors declare that they have no known competing financial interests or personal relationships that could have appeared to influence the work reported in this paper.

Data availability

The data from this study can be made available upon reasonable request.

References

[1] Van Criekinge T, Saeys W, Hallemans A, Velghe S, Viskens P-J, Vereeck L, et al. Trunk biomechanics during hemiplegic gait after stroke: a systematic review. Gait Posture 2017;54:133–43. http://dx.doi.org/10.1016/j.gaitpost.2017.03.004.

[2] Milosevic M, Masani K, Kuipers MJ, Rahouni H, Verrier MC, McConville KMV, et al. Trunk control impairment is responsible for postural instability during quiet sitting in individuals with cervical spinal cord injury. Clin Biomech 2015;30(5):507–12. http://dx.doi.org/10.1016/j.clinbiomech.2015.03.002.

[3] Van der Heide JC, Hadders-Algra M. Postural muscle dyscoordination in children with cerebral palsy. Neural Plast 2005;12(2–3):197–203. http://dx.doi.org/10.1155/NP.2005.197.

[4] Dietz V, Fouad K. Restoration of sensorimotor functions after spinal cord injury. Brain 2014;137(3):654–67. http://dx.doi.org/10.1093/brain/awt262.

[5] Sheng L. Spasticity, motor recovery, and neural plasticity after stroke. Front Neurol 2017;8. http://dx.doi.org/10.3389/fneur.2017.00120.

[6] Anderson KD. Targeting recovery: priorities of the spinal cord-injured population. J Neurotrauma 2004;21(10):1371–83. http://dx.doi.org/10.1089/neu.2004.21.1371.

[7] Verheyden G, Nieuwboer A, Wit LD, Feys H, Schuback B, Baert I, et al. Trunk performance after stroke: an eye catching predictor of functional outcome. J Neurol Neurosurg Psychiatry 2007;78(7):694–8. http://dx.doi.org/10.1136/jnnp.2006.101642.

[8] Borghuis J, Hof AL, Lemmink KAPM. The importance of sensory-motor control in providing core stability. Sport Med 2008;38(11):893–916. http://dx.doi.org/10.2165/00007256-200838110-00002.

[9] Abdollahi F, Farshchiansadegh A, Pierella C, Seáñez González I, Thorp E, Lee MH, et al. Body-machine interface enables people with cervical spinal cord injury to control devices with available body movements: proof of concept. Neurorehabil Neural Repair 2017;31(5):487–93. http://dx.doi.org/10.1177/1545968317693111.

[10] Pierella C, Abdollahi F, Farshchiansadegh A, Pedersen J, Thorp EB, Mussa-Ivaldi FA, et al. Remapping residual coordination for controlling assistive devices and recovering motor functions. Neuropsychologia 2015;79(Pt B):364–76. http://dx.doi.org/10.1016/j.neuropsychologia.2015.08.024.

[11] Casadio M, Ranganathan R, Mussa-Ivaldi FA. The body-machine interface: a new perspective on an old theme. J Mot Behav 2012;44(6):419–33. http://dx.doi.org/10.1080/00222895.2012.700968.

[12] Miehlbradt J, Cherpillod A, Mintchev S, Coscia M, Artoni F, Floreano D, et al. Data-driven body–machine interface for the accurate control of drones. Proc Natl Acad Sci USA 2018;115(31):7913–8. http://dx.doi.org/10.1073/pnas.1718648115.

[13] Freccero A, Feder M, Grioli G, Catalano MG, Massone A, Bicchi A, et al. A body–machine interface for assistive robot control in spinal cord injury: system description and preliminary tests. Appl Sci 2025;15(4):1792. http://dx.doi.org/10.3390/app15041792.

[14] Pierella C, Pellegrino L, Muller M, Coscia M, Inglese M, Solaro C, et al. EMG based body-machine interface for adaptive and personalized robotic training of persons with multiple sclerosis. In: 2022 9th IEEE BioRob. IEEE Press; 2022, p. 1–6. http://dx.doi.org/10.1109/BioRob52689.2022.9925509.

[15] Mugler EM, Tomic G, et al. Myoelectric computer interface training for reducing co-activation and enhancing arm movement in chronic stroke survivors: a randomized trial. Neurorehabil Neural Repair 2019;33(4). http://dx.doi.org/10.1177/1545968319834903.

[16] Pierella C, Dhanasekaran A, Carlini G, Coduri M, Marchesi G, Casadio M. BridGE: a new system to train selective pelvis movements. IEEE Access 2023;PP. http://dx.doi.org/10.1109/ACCESS.2023.3328206, 1–1.

[17] Summa S, Pierella C, Giannoni P, Sciacchitano A, Iacovelli S, Farshchiansadegh A, et al. A body-machine interface for training selective pelvis movements in stroke survivors: a pilot study. In: 2015 37th annual international conference of the IEEE EMBC. 2015, p. 4663–6. http://dx.doi.org/10.1109/EMBC.2015.7319434.

[18] Wolpert D, Diedrichsen J, Flanagan JR. Principles of sensorimotor learning. Nat Rev Neurosci 2011;12(11):739–51. http://dx.doi.org/10.1038/nrn3112.

[19] Iuppariello L, Bifulco P, Romano M, D'Addio G, Cesarelli M. A hybrid decomposition method to infer the sub-movements composition of planar reaching movements. Inf Med Unlocked 2017;9:210–8. http://dx.doi.org/10.1016/j.imu.2017.09.004.

[20] Murphy JO, Audu ML, Lombardo LM, Foglyano KM, Triolo RJ. Feasibility of closed-loop controller for righting seated posture after spinal cord injury. J Rehabil Res Dev 2014;51(5):747–60. http://dx.doi.org/10.1682/JRRD.2013.09.0200.

[21] De Luca A, Squeri V, Barone LM, Vernetti Mansin H, Ricci S, Pisu I, et al. Dynamic stability and trunk control improvements following robotic balance and core stability training in chronic stroke survivors: a pilot study. Front Neurol 2020;11:494. http://dx.doi.org/10.3389/fneur.2020.00494.

[22] Herrera V, Albusac J, Angulo E, González-Morcillo C, de Los Reyes-Guzman A, Vallejo D. Virtual reality-assisted goalkeeper training for upper limb rehabilitation in a safe and adapted patient environment. IEEE Access 2024;12:194256–79. http://dx.doi.org/10.1109/ACCESS.2024.3519731.

[23] Cheung VC, Turolla A, Agostini M, Silvoni S, Bennis C, Kasi P, et al. Muscle synergy patterns as physiological markers of motor cortical damage. Proc Natl Acad Sci USA 2012;109(36):14652–6. http://dx.doi.org/10.1073/pnas.1212056109.

[24] Rizzoglio F, Sciandra F, Galofaro E, Losio L, Quinland E, Leoncini C, et al. A myoelectric computer interface for reducing abnormal muscle activations after spinal cord injury. In: IEEE int conf rehabil robot. 2019, p. 1049–54. http://dx.doi.org/10.1109/ICORR.2019.8779493.

[25] Balbinot G, Li G, Wiest MJ, Pakosh M, Furlan JC, Kalsi-Ryan S, et al. Properties of the surface electromyogram following traumatic spinal cord injury: a scoping review. J Neuroeng Rehabil 2021;18(1):105. http://dx.doi.org/10.1186/s12984-021-00888-2.

[26] Middaugh SJ. On clinical efficacy: why biofeedback does–and does not–work. Biofeedback Self Regul 1990;15(3):191–208. http://dx.doi.org/10.1007/BF01011105.

[27] Liu R, Song Q, Ma T, Pan H, Li H, Zhao X. SoftBoMI: a non-invasive wearable body–machine interface for mapping movement of shoulder to commands. J Neural Eng 2024;21(6):066007. http://dx.doi.org/10.1088/1741-2552/ad8b6e.

[28] Brucker BS, Bulaeva NV. Biofeedback effect on electromyography responses in patients with spinal cord injury. Arch Phys Med Rehabil 1996;77(2):133–7. http://dx.doi.org/10.1016/s0003-9993(96)90157-4.

[29] Pierella C, D'Antuono C, Marchesi G, Menotti CE, Casadio M. A computer interface controlled by upper limb muscles: effects of a two weeks training on younger and older adults. IEEE Trans Neural Syst Rehabil Eng 2023;31:3744–51. http://dx.doi.org/10.1109/TNSRE.2023.3312981.

[30] Verros S, Lucassen K, Hekman EE, Bergsma A, Verkerke GJ, Koopman BF. Evaluation of intuitive trunk and non-intuitive leg sEMG control interfaces as command input for a 2-D Fitts's law style task. PLoS One 2019;14(4):e0214645. http://dx.doi.org/10.1371/journal.pone.0214645.

[31] Seo G, Kishta A, Mugler E, et al. Myoelectric interface training enables targeted reduction in abnormal muscle co-activation. J Neuroeng Rehabil 2022;19(1):67. http://dx.doi.org/10.1186/s12984-022-01045-z.

[32] Wright ZA, Rymer WZ, Slutzky MW. Reducing abnormal muscle coactivation after stroke using a myoelectric-computer interface: a pilot study. Neurorehabil Neural Repair 2014;28(5):443–51. http://dx.doi.org/10.1177/1545968313517751.

[33] Bigoni M, Cimolin V, Vismara L, Tarantino AG, Baudo S, Trotti C, et al. Retraining selective trunk muscle activity: a key to more successful rehabilitation outcomes for hemiparetic stroke patients. NeuroRehabilitation 2021;49(1):87–94. http://dx.doi.org/10.3233/NRE-210094.

[34] Pierella C, Sciacchitano A, Farshchiansadegh A, Casadio M, Mussa-Ivaldi SA. Linear vs non-linear mapping in a body machine interface based on electromyographic signals. In: 2018 7th IEEE BioRob. 2018, p. 162–6. http://dx.doi.org/10.1109/BIOROB.2018.8487185.

[35] Rizzoglio F, Pierella C, De Santis D, Mussa-Ivaldi F, Casadio M. A hybrid body-machine interface integrating signals from muscles and motions. J Neural Eng 2020;17(4):046004. http://dx.doi.org/10.1088/1741-2552/ab9b6c.

[36] Lee J, Gebrekristos T, De Santis D, Nejati-Javaremi M, Gopinath D, Parikh B, et al. Learning to control complex robots using high-dimensional body–machine interfaces. ACM Trans Hum Robot Interact 2024;13(3):38. http://dx.doi.org/10.1145/3630264.

[37] Guidolin M, Menegatti E, Reggiani M, Tagliapietra L. A ROS driver for Xsens wireless inertial measurement unit systems. In: IEEE int conf ind technol. ICIT, 2021, p. 677–83. http://dx.doi.org/10.1109/ICIT46573.2021.9453640.

[38] McGill S, Juker D, Kropf P. Appropriately placed surface EMG electrodes reflect deep muscle activity (psoas, quadratus lumborum, abdominal wall) in the lumbar spine. J Biomech 1996;29(11):1503–7. http://dx.doi.org/10.1016/0021-9290(96)84547-7.

[39] Wang Y-J, Li J-J, Zhou H-J, Liu G-L, Zheng Y, Wei B, et al. Surface electromyography as a measure of trunk muscle activity in patients with spinal cord injury: a meta-analytic review. J Spinal Cord Med 2016;39(1):15–23. http://dx.doi.org/10.1179/2045772315Y.0000000059.

[40] Redfern M, Hughes R, Chaffin D. High-pass filtering to remove electrocardiographic interference from torso EMG recordings. Clin Biomech (Bristol) 1993;8(1):44–8. http://dx.doi.org/10.1016/S0268-0033(05)80009-9.

[41] Bi L, Feleke AG, Guan C. A review on EMG-based motor intention prediction of continuous human upper limb motion for human-robot collaboration. Biomed Signal Process Control 2019;51:113–27. http://dx.doi.org/10.1016/j.bspc.2019.02.011.

[42] Khadivar F, Mendez V, Correia C, Batzianoulis I, Billard A, Micera S. EMG-driven shared human-robot compliant control for in-hand object manipulation in hand prostheses. J Neural Eng 2022;19(6):066024. http://dx.doi.org/10.1088/1741-2552/aca35f.

[43] Samarasinghe S. Neural networks for applied sciences and engineering: From fundamentals to complex pattern recognition. New York: Auerbach Publications; 2007, http://dx.doi.org/10.1201/9780849333750.

[44] Bishop CM, Nasrabadi NM. Pattern recognition and machine learning, vol. 4, Springer; 2006.

[45] Xiong D, Zhang D, Zhao X, Zhao Y. Deep learning for EMG-based human-machine interaction: a review. IEEE/CAA J Autom Sin 2021;8(3):512–33. http://dx.doi.org/10.1109/JAS.2021.1003865.

[46] Hochreiter S, Schmidhuber J. Long short-term memory. Neural Comput 1997;9(8):1735–80. http://dx.doi.org/10.1162/neco.1997.9.8.1735.

[47] Liu J, Kang SH, Xu D, Ren Y, Lee SJ, Zhang L-Q. EMG-based continuous and simultaneous estimation of arm kinematics in able-bodied individuals and stroke survivors. Front Neurosci 2017;11:480. http://dx.doi.org/10.3389/fnins.2017.00480.

[48] Lee H, Kim D, Park Y-L. Explainable deep learning model for EMG-based finger angle estimation using attention. IEEE Trans Neural Syst Rehabil Eng 2022;30:1877–86. http://dx.doi.org/10.1109/TNSRE.2022.3188275.

[49] Quivira F, Koike-Akino T, Wang Y, Erdogmus D. Translating sEMG signals to continuous hand poses using recurrent neural networks. In: 2018 IEEE EMBS int conf biomed health inform. BHI, IEEE; 2018, p. 166–9. http://dx.doi.org/10.1109/BHI.2018.8333395.

[50] Truong MTN, Ali AEA, Owaki D, Hayashibe M. EMG-based estimation of lower limb joint angles and moments using long short-term memory network. Sensors (Basel) 2023;23(6):3331. http://dx.doi.org/10.3390/s23063331.

[51] Van der Kooij H, van Asseldonk E, van der Helm FC. Comparison of different methods to identify and quantify balance control. J Neurosci Methods 2005;145(1–2):175–203. http://dx.doi.org/10.1016/j.jneumeth.2005.01.003.

[52] Moorhouse KM, Granata KP. Trunk stiffness and dynamics during active extension exertions. J Biomech 2005;38(10):2000–7. http://dx.doi.org/10.1016/j.jbiomech.2004.09.014.

[53] Soangra R, Sivakumar R, Anirudh ER, Reddy YSV, John EB. Evaluation of surgical skill using machine learning with optimal wearable sensor locations. PLoS One 2022;17(6):e0267936. http://dx.doi.org/10.1371/journal.pone.0267936.

[54] Liesefeld HR, Janczyk M. Combining speed and accuracy to control for speed-accuracy trade-offs(?). Behav Res Methods 2019;51:40–60. http://dx.doi.org/10.3758/s13428-018-1076-x.

[55] Rabiner L, Juang B-H. Fundamentals of speech recognition. Englewood Cliffs, N.J.: PTR Prentice Hall; 1993.

[56] Semblantes PA, Andaluz VH, Lagla J, Chicaiza FA, Acurio A. Visual feedback framework for rehabilitation of stroke patients. Inf Med Unlocked 2018;13:41–50. http://dx.doi.org/10.1016/j.imu.2018.10.002.

[57] Gaspar M, Welke B, Seehaus F, Hurschler C, Schwarze M. Dynamic time warping compared to established methods for validation of musculoskeletal models. J Biomech 2017;55:156–61. http://dx.doi.org/10.1016/j.jbiomech.2017.02.025.

[58] Geiger DE, Behrendt F, Schuster-Amft C. EMG muscle activation pattern of four lower extremity muscles during stair climbing, motor imagery, and robot-assisted stepping: a cross-sectional study in healthy individuals. Biomed Res Int 2019;2019:9351689. http://dx.doi.org/10.1155/2019/9351689, 8 pages.

[59] Lee DC, Lim HK, McKay WB, Priebe MM, Holmes SA, Sherwood AM. Toward an objective interpretation of surface EMG patterns: a voluntary response index (vri). J Electromyogr Kinesiol 2004;14(3):379–88. http://dx.doi.org/10.1016/j.jelekin.2003.10.006.

[60] Kadılar MC, Toptaş E, Akgün G. An EMG-based prosthetic hand design and control through dynamic time warping. Int J Adv Nat Sci Eng Res 2024;8(2):339–49.

[61] Liao C, Liaw L, Wang R, Su F, Hsu A. Electromyography of symmetrical trunk movements and trunk position sense in chronic stroke patients. J Phys Ther Sci 2015;27(9):2675–81. http://dx.doi.org/10.1589/jpts.27.2675.

[62] Dickstein R, Shefi S, Marcovitz E, Villa Y. Electromyographic activity of voluntarily activated trunk flexor and extensor muscles in post-stroke hemiparetic subjects. Clin Neurophysiol 2004;115(4):790–6. http://dx.doi.org/10.1016/j.clinph.2003.11.018.

[63] Cui H, Zhong W, Yang Z, Cao X, Dai S, Huang X, et al. Comparison of facial muscle activation patterns between healthy and Bell's palsy subjects using high-density surface electromyography. Front Hum Neurosci 2021;14. http://dx.doi.org/10.3389/fnhum.2020.618985.

[64] Talebian S, Hosseini M, Bagheri H, Olyaei GR, Reazasoltani A. Trunk muscle fatigue in subjects with a history of low back pain and a group of healthy controls measured by similarity index. J Back Musculoskelet Rehabil 2011;24:17–22. http://dx.doi.org/10.3233/BMR-2011-0270.

[65] Del Vecchio A, Casolo A, Negro F, Scorcelletti M, Bazzucchi I, Enoka R, et al. The increase in muscle force after 4 weeks of strength training is mediated by adaptations in motor unit recruitment and rate coding. J Physiol 2019;597(7):1873–87. http://dx.doi.org/10.1113/JP277250.

[66] Misgeld BJE, Lüken M, Heitzmann D, Wolf SI, Leonhardt S. Body-sensor-network-based spasticity detection. IEEE J Biomed Heal Inf 2016;20(3):748–55. http://dx.doi.org/10.1109/JBHI.2015.2477245.

[67] Ma K, Chen Y, Zhang X, Zheng H, Yu S, Cai S, et al. sEMG-based trunk compensation detection in rehabilitation training. Front Neurosci 2019;13:1250. http://dx.doi.org/10.3389/fnins.2019.01250.

[68] De Santis D. A framework for optimizing co-adaptation in body-machine interfaces. Front Neurorobot 2021;15. http://dx.doi.org/10.3389/fnbot.2021.662181.